Structure
Article

Crystallographic and Functional Analysis of the ESCRT-I /HIV-1 Gag PTAP Interaction

Young Jun Im,[1,5] Lillian Kuo,[2] Xuefeng Ren,[1] Patricia V. Burgos,[3,6] Xue Zhi Zhao,[4] Fa Liu,[4] Terrence R. Burke, Jr.,[4] Juan S. Bonifacino,[3] Eric O. Freed,[2] and James H. Hurley[1,*]
[1]Laboratory of Molecular Biology, National Institute of Diabetes and Digestive and Kidney Diseases, National Institutes of Health, Bethesda, MD 20892-0580, USA
[2]HIV Drug Resistance Program, CCR, NCI-Frederick, Frederick, MD 21702, USA
[3]Cell Biology and Metabolism Program, Eunice Kennedy Shriver National Institute of Child Health and Development, NIH, Bethesda, MD, 20892, USA
[4]Chemical Biology Laboratory, Molecular Discovery Program, CCR, NCI-Frederick, Frederick, MD 21702, USA
[5]Present address: College of Pharmacy, Chonnam National University, 77 Yongbongro, Bukgu, Gwangju City 500-757 South Korea
[6]Present address: Department of Physiology, Universidad Austral de Chile, Valdivia 509-9200, Chile
*Correspondence: hurley@helix.nih.gov
DOI 10.1016/j.str.2010.08.010

SUMMARY

Budding of HIV-1 requires the binding of the PTAP late domain of the Gag p6 protein to the UEV domain of the TSG101 subunit of ESCRT-I. The normal function of this motif in cells is in receptor downregulation. Here, we report the 1.4–1.6 Å structures of the human TSG101 UEV domain alone and with wild-type and mutant HIV-1 PTAP and Hrs PSAP nonapeptides. The hydroxyl of the Thr or Ser residue in the P(S/T)AP motif hydrogen bonds with the main chain of Asn69. Mutation of the Asn to Pro, blocking the main-chain amide, abrogates PTAP motif binding in vitro and blocks budding of HIV-1 from cells. N69P and other PTAP binding-deficient alleles of TSG101 did not rescue HIV-1 budding. However, the mutant alleles did rescue downregulation of endogenous EGF receptor. This demonstrates that the PSAP motif is not rate determining in EGF receptor downregulation under normal conditions.

INTRODUCTION

Most membrane-enveloped animal viruses, including HIV-1, require the assistance of the host Endosomal Sorting Complex Required for Transport (ESCRT) machinery in order for nascent virions to be severed from the host cell membrane (Bieniasz, 2009; Chen and Lamb, 2008; Morita and Sundquist, 2004). The normal functions of the ESCRT complexes are in the sorting of ubiquitinated transmembrane proteins (Raiborg and Stenmark, 2009), the budding of cargo-rich membrane patches into the lumen of the endosomes (Hurley and Hanson, 2010; Wollert and Hurley, 2010), and the severing of the narrow membrane necks (Hurley and Hanson, 2010; Wollert et al., 2009). The initial recognition and clustering of ubiquitinated receptors is primarily the task of ESCRT-0 (Hurley and Hanson, 2010; Wollert and Hurley, 2010), bud formation the task of ESCRT-I and –II (Wollert and Hurley, 2010), and neck severing is carried out by ESCRT-III (Wollert et al., 2009). All of these steps are required for the normal functioning of the ESCRT pathway in receptor downregulation, but only the membrane neck severing step appears to be required for viral budding (McDonald and Martin-Serrano, 2009). So far as is known, no virus directly recruits the ESCRT-III membrane scission machinery. Rather, viral proteins recruit various ESCRT components via short peptide motifs known as late domains (Freed, 2002). There are three major classes of late domains, of the form PPXY, YPX_nL, and P(S/T)AP. The most widespread of the late domains is the P(S/T)AP motif, which binds to the ubiquitin E2 variant (UEV) domain of the TSG101 subunit of ESCRT-I. The Gag p6 protein of HIV-1 contains a single PTAP motif whose presence and binding to TSG101 is essential for efficient viral budding (Demirov et al., 2002a, 2002b; Garrus et al., 2001; Martin-Serrano et al., 2001; VerPlank et al., 2001). A single PSAP motif in the Hrs subunit of ESCRT-0 has also been shown to bind to the TSG101 UEV domain (Bache et al., 2003; Lu et al., 2003; Pornillos et al., 2003).

The ESCRT-I complex is a 1:1:1:1 heterotetramer of the subunits TSG101 (Vps23 in yeast), VPS28, VPS37, and MVB12 (Audhya et al., 2007; Morita et al., 2007). In humans, there are four well-established isoforms of VPS37 and two of MVB12 (Morita et al., 2007). TSG101 contains at its N terminus an UEV domain, an enzymatically inactive variant of an ubiquitin E2 enzyme. The UEV domain of TSG101 is attached by a ~50 residue Pro-rich linker to one end of the rigid 180 Å long ESCRT-I core (Kostelansky et al., 2007). In addition to binding to the P(S/T)AP motif, the UEV domain also binds to ubiquitin at a nonoverlapping site (Sundquist et al., 2004; Teo et al., 2004). The solution structure of the UEV complex with the HIV-1 PTAP peptide has been invaluable as the structural underpinning for P(S/T)XP late domain activity. However, this structure does not explain certain key aspects of the structure-activity relationships. A Ser or Thr is always present at the second position in the motif, and its presence is required for binding (Garrus et al., 2001; Martin-Serrano et al., 2001; Schlundt et al., 2009) and function (Huang et al., 1995; Martin-Serrano et al., 2001). However, the Thr hydroxyl in the NMR structure is pointed toward solution and makes no hydrogen bonds with the protein.

Current anti-HIV-1 therapies for treating AIDS primarily target the three viral enzymes reverse transcriptase, protease, and integrase. Despite the effectiveness of these therapies, strains

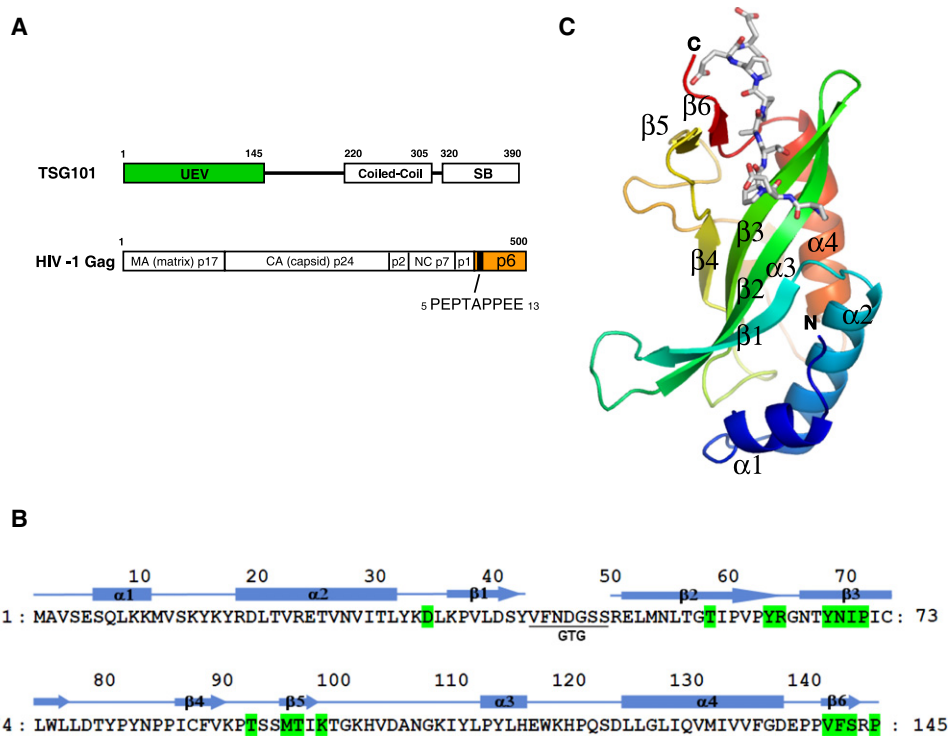

Figure 1. Structure of TSG101 UEV and HIV-1 p6 Peptide

(A) Schematic representations of human TSG101 and HIV-1 Gag. Abbreviations within TSG101 are UEV (ubiquitin E2 variant) and SB ("steadiness" box). Viral protease cleavage sites are indicated by vertical lines and the names of resulting proteins are shown. The location of the PTAP peptide in $p6^{Gag}$ is indicated.

(B) Amino acid sequence and secondary structure of TSB101 UEV. The residues involved in PTAP peptide binding are colored in green.

(C) Overall structure of TSG101 UEV and HIV p6 peptide.

resistant to inhibitors of all three of the HIV-encoded enzymes have been isolated (Shafer and Schapiro, 2008). Much of the effort invested in mechanistic studies of the ESCRT system has been motivated by the long-term need to develop new potential therapeutic targets, given the likelihood that HIV-1 will evolve in future years to evade current treatments. Although it is more difficult to inhibit peptide-protein interactions than to block enzyme activity, the PTAP-TSG101 interaction remains the most promising potential therapeutic target involving the budding step of the viral life cycle (Liu et al., 2008; Tavassoli et al., 2008; Waheed and Freed, 2008). Indeed, stable expression in culture of a dominant-negative fragment of TSG101 blocks the replication of feline immunodeficiency virus (FIV), a lentivirus that like HIV-1 uses a P(S/T)AP-TSG101 interaction to bud from cells (Luttge et al., 2008).

Despite the interest in targeting the p6-TSG101 interaction as a novel antiviral strategy, prospects have been clouded by concerns that this same interaction is involved in the normal function of TSG101 in receptor downregulation. TSG101 was originally described as a tumor susceptibility gene (Li and Cohen, 1996), and loss of TSG101 leads to tumors in *Drosophila* (Moberg et al., 2005). It has been widely assumed that the binding of human ESCRT-I with ESCRT-0 (Bache et al., 2003; Lu et al., 2003; Pornillos et al., 2003) would be critical for the downregulation of proliferative receptors such as EGF receptor (EGFR), and this concern has to some extent deterred efforts to target this interaction for therapeutic purposes. However, conflicting reports have been presented on the requirement of this interaction for EGFR downregulation (Demirov et al., 2002a; Lu et al., 2003). Because of the uncertainties concerning the structural details of the complex and the effect of its disruption on EGFR downregulation, we obtained high-resolution crystal structures of the TSG101 UEV domain with and without P(S/T)AP-containing peptides and reexamined its functions using RNAi knockdown/rescue experiments. The high-resolution crystal structures were used to design RNAi-resistant alleles coding for mutants selectively impaired in P(S/T)AP motif binding to the UEV domain. The results show that the PTAP-UEV interaction is required for HIV-1 budding, as expected. However, we found that the interaction is not a rate-limiting step in EGFR downregulation. Challenges also remain in the design of pharmacologically effective inhibitors to block protein-peptide binding. Having in hand high-resolution structures of the complex to be targeted will be a valuable addition to the tool kit for the challenging but important goal of PTAP inhibitor design.

RESULTS

Structure of the HIV-1 Gag PTAP Peptide-UEV Domain Complex

In order to obtain crystals of the UEV domain (Figure 1A) in complex with peptides, the six residue loop between β1 and β2, which is flexible in the absence of bound ubiquitin, was replaced by the linker Gly-Thr-Gly (Figure 1B). The deletion does

Table 1. Statistics of Data Collection and Crystallographic Refinement

Crystal	HRS (residues 346–354) PTPSAPVPL	Apo UEV	Wild-type HIV-1 Gag PEPTAPPEE	P7A Mutant HIV-1 Gag PEATAPPEE
Constructs	TSG101 (2–145)	TSG101 (2–145)	TSG101 (2–145)	TSG101 (2–145)
	43–48 GTG	43–48 GTG	43–48 GTG	43–48 GTG
Space group, unit cell	$P2_12_12_1$	$P2_1$	$P2_12_12_1$	$P2_12_12_1$
	a = 33.6 Å, b = 45.1 Å,	a = 33.6 Å, b = 45.7 Å,	a = 33.5 Å, b = 45.8 Å,	a = 33.5 Å, b = 45.8 Å,
	c = 87.7 Å	c = 50.2 Å β = 108.3	c = 85.4 Å	c = 89.0 Å
X-ray source	APS 22-ID	APS 22-ID	APS 22-BM	APS 22-ID
Wavelength (Å)	1.0000	1.0000	1.0000	1.0000
Resolution (Å) (last shell)	1.4 (1.40–1.42)	1.5 (1.50–1.53)	1.6 (1.60–1.63)	1.6 (1.60–1.63)
No. of unique reflections	25,924	22,570	17,689	18,234
I/σ(I)σ (last shell)	28.9 (3.6)	47.5 (25.3)	30.4 (4.1)	25.3 (6.6)
Rsym (%)	6.3 (34.3)	3.9 (9.2)	7.6 (32.8)	6.3 (23.2)
Data completeness (%)	96.1 (97.3)	97.1 (96.2)	98.8 (93.5)	97.1 (90.5)
Refinement				
R factor (%)	20.7 (24.1)	21.5 (21.0)	19.9 (24.0)	20.6 (21.9)
Free R factor (%)	22.4 (24.5)	23.2 (22.8)	23.5 (27.8)	23.0 (27.4)
Rms bond length (Å)	0.005	0.005	0.005	0.005
Rms bond angle (°)	1.3	1.3	1.3	1.3
Average B value (Å^2)	15.8	15.2	17.8	15.6
Number of atoms	Protein 1195; water 214	Protein 1121; water 217	Protein 1207; water 156	Protein 1193; water 125

not appear to have affected the overall structure, as the 1.5 Å resolution structure of the unliganded loop deletion construct is essentially superimposable on the 2.26 Å resolution X-ray structure of the wild-type unliganded UEV domain (Palencia et al., 2006). The superposition has an rmsd of 0.5 Å for 122 Ca positions, including the entire domain except for the β1/β2 linker and the extreme C terminus. The structure of the human TSG101 UEV domain bound to the HIV-1 Gag p6 nonapeptide PEPTAPPEE was determined at 1.6 Å resolution by molecular replacement with the unliganded wild-type UEV (Palencia et al., 2006) (Figure 1C and Table 1). The HIV-1 Gag PTAP peptide binds to a groove on the UEV domain formed between the β2/β3 hairpin, the β4/β5 loop, and the C-terminal residues, in the same orientation as seen previously in the solution NMR analysis (Pornillos et al., 2002a).

The entire HIV-1 p6 nonapeptide is well ordered and visualized in the binding groove (Figure 2A). Every residue of the peptide makes contact with the UEV domain via either the main chain, side chain, or both (Figures 2B and 2C), with the possible exception of the first residue, Pro5. Contact distances with Pro5 are on the borderline of significance. The main-chain carbonyl of Glu6 hydrogen bonds to the side chain of Asn69, although at 3.3 Å and exposed to solvent, the energetic contribution of this interaction is probably marginal. The first residue of the PTAP motif, Pro7, is wedged in a shallow hydrophobic pocket formed by the side chains of Thr58, Pro71, and Thr92. Both Thr residues contribute their γ-methyl groups to the pocket, and their hydroxyl groups point away from it. The Pro7 pocket is open on the side corresponding to the N terminus of the peptide, leaving the Pro7 side chain partially exposed to solvent. The main-chain amide of the critical motif residue Thr8 forms a hydrogen bond with the main-chain carbonyl of Asn69. The side-chain hydroxyl group of Thr8 forms a relatively short 2.8 Å hydrogen bond with the main-chain amide of Asn69. The γ-methyl of the Thr8 side chain points toward solvent and has no direct interactions with the domain, however. The methyl group of the conserved Ala9 side chain is buried in a tightly packed pocket formed by the side chains of Ile70, Met95, and Val141. The tight packing around the Ala side chain explains the critical requirement for an Ala at this position in the motif. The Ala main-chain carbonyl makes a 2.6 Å hydrogen bond to the side chain of Ser143. The side chain of the last conserved motif residue, Pro10, is almost completely buried in a deep hydrophobic pocket. The floor of the pocket is formed by the side chain of Pro139, while the walls are formed by the side chains of Tyr63, Tyr68, and Phe142. The Pro10 main-chain carbonyl forms a hydrogen bond with the main-chain amide of Ser143. The side chain of Pro11 comes within 3.7 Å of the side chain of Tyr68. The side chains of Glu12 and Glu13 are in the vicinity of the basic side chains of Lys98 and Arg64, respectively, though these residues are highly solvated and probably contribute only marginally to binding affinity.

Conformational Changes Induced by Peptide Binding

The high-resolution structure determination of both the HIV-1 PEPTAPPEE complex and the unliganded UEV structure using the same UEV construct allows a detailed analysis of structural changes on binding. These changes are modest in magnitude. The largest change is a rotamer shift in the phenyl side chain of Phe142 such that it makes contact with Pro10 (Figure 2D). The Phe142 side-chain atoms move by as much as 8 Å in this shift, thereby creating the binding pocket for Pro10 by induced fit. The C-terminal residues Arg144 and

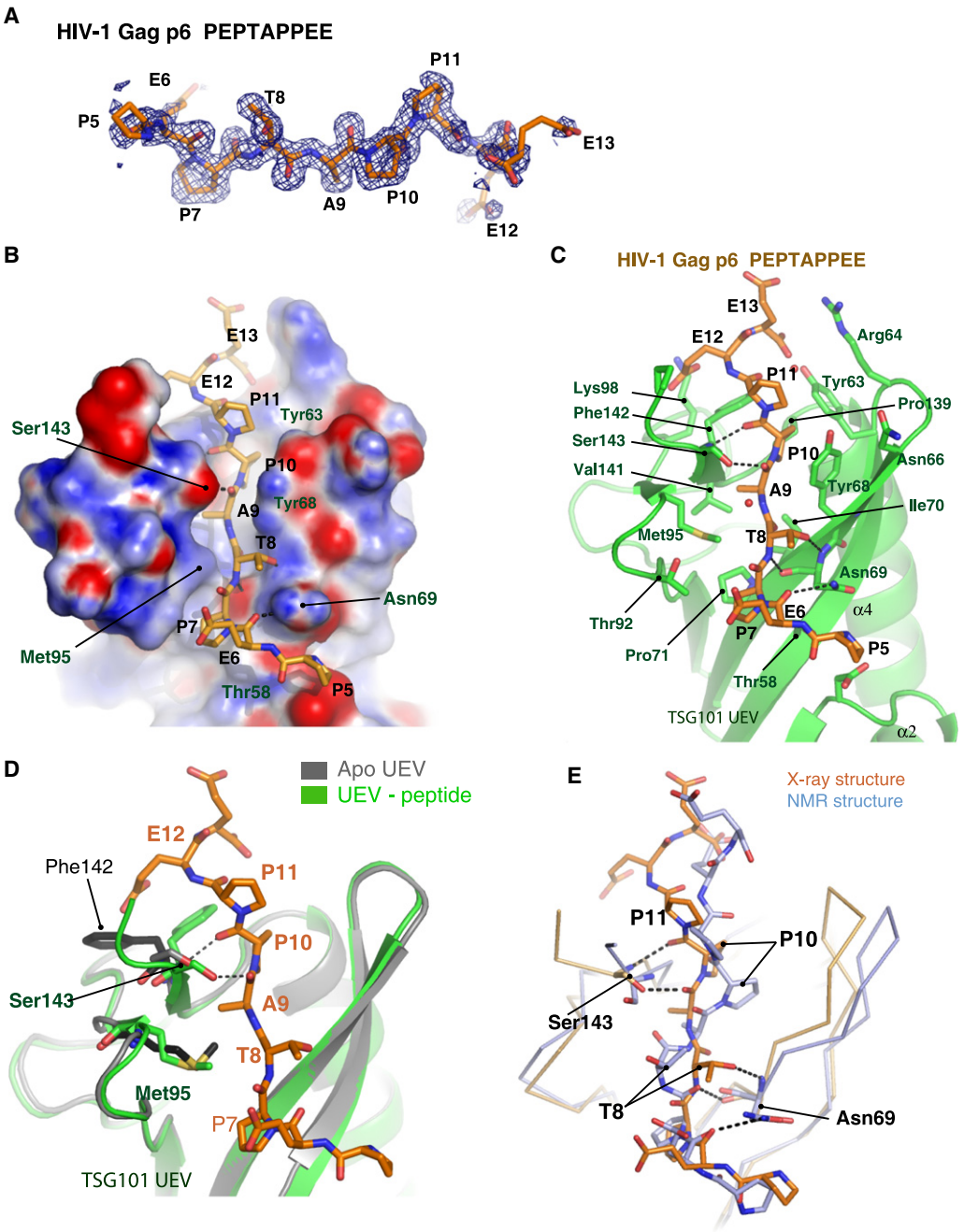

Figure 2. Binding of HIV-1 PTAP Peptide

(A) 1.6 Å simulated-annealing omit map of the HIV-1 PTAP peptide with the final model superimposed.

(B) Electrostatic surface representation of the UEV-HIV peptide. The electrostatic surface was colored using APBS tools of PyMOL software.

(C) A ball and stick representation of the PTAP peptide binding.

(D) Structural superposition of apo UEV and HIV-1 PTAP peptide complex.

(E) Structural comparison of X-ray structure (this study) and the NMR structure (PDB id: 1M4Q) of TSG101 UEV-HIV PTAP complex.

Pro145 of the UEV domain are only ordered well enough to model in the peptide complex, not in the unliganded structure. For residues 142-143, B factors drop from the 25–40 $Å^2$ range to the 12–18 $Å^2$ for the peptide complex. The side chain of Met95 moves by a maximum of 2 Å, and the B factors drop from the range of 33–43 to 14–21 $Å^2$.

Comparison of Crystal and Solution NMR Structures of the HIV-1 Peptide Complex

As would be expected for a solution NMR/X-ray crystallographic comparison, the Cα rmsd of 1.6 Å between the 126 most similar Cα positions of the two structure is substantially higher than that between crystal structures of the UEV domain

in different ligation states and crystal forms and from different constructs (0.4–0.5 Å for ~140 Cα positions). The largest differences in the path of the main chain, of up to 7 Å, are in the β1/β2 (also influenced by the loop deletion construct), β3/β4, and α3/α4 loops, which are all distal to the peptide binding site. Near the peptide-binding site, all Cα positions are within 2 Å in of each other in the overlaid structures, and most are closer. Within the peptide-binding pocket, the van der Waals contacts around the Pro7 side chain are essentially the same in both structures. Indeed, throughout the peptide-binding site, the qualitative conclusions about the identity of van der Waals interaction partners drawn from the NMR structure are consistent with the X-ray structure. In the NMR analysis, the Thr 8 hydroxyl proton resonance was observed, showing that it is protected from solvent exchange (Pornillos et al., 2002a), and consistent with a strong and stable hydrogen-bonding interaction. The hydrogen-bonding partner of the Thr8 side chain could not be identified directly from the spectra (Pornillos et al., 2002a). It was inferred from the derived structures that Thr 8 might donate a hydrogen bond to the backbone carbonyl of Arg 144 and accept one from the O of Ser 143 (Pornillos et al., 2002a). However, these interactions were not observed in all calculated structures because the Ser 143 and Arg 144 positions were not precisely defined by the NOE data (Pornillos et al., 2002a). The Pornillos et al. (2002a) study notes that the nature of the hydrogen bond of the hydroxyl is not resolved by the NMR analysis.

Overall, the main difference between the two structures is in the conformation of the central portion of the peptide. The peptide group connecting Pro7 and Thr8 is flipped 180° between the crystal and the averaged NMR structure (Figure 2E), thus the hydrogen bonds involving this peptide group and the Thr side chain are not apparent in the solution structure. The peptide connecting Thr8 and Ala9 is also in a sharply different orientation. The conserved residues of the motif have a regular β-conformation in the X-ray structure, while the peptide is sharply kinked about the Thr residue in the NMR structure. Most of the key hydrogen-bonding interactions were therefore missed in the NMR analysis. The improved accuracy of the high-resolution X-ray analysis permits the hydrogen bond network to be described for the first time.

Structure of the ESCRT-0 Subunit Hrs PSAP Motif Peptide-UEV Domain Complex

The Hrs PSAP motif nonapeptide corresponding to residues 346-354 of human Hrs binds in the same overall geometry as the HIV-1 peptide (Figures 3A and 3B). The replacement of the HIV-1 Glu6 by Hrs Thr347 causes essentially no change in the structure, as both side chains point toward solvent. Likewise, the replacement of HIV-1 Thr8 by Hrs Ser has no effect on the structure, since the γ-methyl of the Thr8 points toward solvent. The key Ala and final Pro residues of the motif are in identical positions. The replacement of Pro11 by Val results in the loss of a van der Waals interaction with Tyr68. The only substantial structural changes are seen at the C-terminal end of the peptide, where Glu12 and Glu13 of HIV-1 Gag are replaced by Pro and Leu in Hrs. The Hrs Pro forms a new contact that pushes the C-terminal Pro145 of the UEV domain away from its position in the HIV-1 complex by 1.5 Å. The loss of the acidic Glu13 at the C terminus of the peptide breaks the charge pair interaction with Arg64. The guanidinium group of the Arg side chain moves 5 Å away from its position in the HIV-1 structure, carrying with it, to a lesser extent, Gly65 and Asn66.

Structure of the HIV-1 P7A Mutant in Complex with the UEV Domain

The replacement of Pro7 by Ala leads to the loss of van der Waals contacts with the γ-methyl groups of Thr58 and Thr92 (Figures 3C and 3D). The comparison of the wild-type and P7A mutant structures shows that the UEV domain structure is identical at these two positions. The UEV structure does not relax at these positions when the contacts are lost, and therefore conformational changes do not mitigate the energetic cost of the lost interactions. Attempts were made to cocrystallize other peptides altered at all of the conserved motif positions, but with the exception of P7A, the rest of the mutant peptides yielded either no crystals or unliganded complexes.

Isothermal Titration Analysis of Binding Determinants

The HIV-1 PTAP nonapeptide bound the UEV domain in solution with a K_d value of 50 μM (Figure 4A and Table 2). This is in reasonable agreement with the value of 27 μM obtained for immobilized GST-p6 residues 1–27 under otherwise similar conditions (Pornillos et al., 2002b). Consistent with previous reports (Pornillos et al., 2002b), the mutants Y63A and M95A, designed to remove van der Waals interactions with the peptide, exhibited sharply reduced and essentially no binding, respectively (Figure 4A and Table 2). The N69P mutant was designed as a key test of the newly described hydrogen bond network model. This mutation was predicted to remove two hydrogen bonds. Of the two, the hydrogen bond between the main-chain amide of Asn69 with the side-chain hydroxyl of Thr8 was judged the more important, hence the choice of Pro as the unique cyclic nature of this side-chain blocks this interaction. We found that the N69P mutation equals M95A in potently blocking binding (Figure 4A and Table 2). Binding of mutants to the Hrs PSAP peptide was not tested, because these mutations are all at sites that interact with the conserved central portion of the peptide common to HIV-1 and Hrs. Therefore the relative effects of the mutations are expected to be identical. The S143A mutant was designed as another test of the role of hydrogen bonding. S143A did not significantly decrease binding. This may be attributable to the very short oxygen-oxygen distance in this hydrogen bond. At 2.6 Å, these atoms are unusually close for a pair in which neither partner is charged, and the resulting steric strain may offset the otherwise favorable energy of the hydrogen bond.

We went on to quantify the effects on affinity of altering the conserved motif residues. The conserved Ala9 of the motif is absolutely required for binding (Figure 4B and Table 2), consistent with its conservation and with peptide screening results (Schlundt et al., 2009). Assuming that the surrounding protein does not relax, the A9G mutation is expected to create an energetically unfavorable cavity the size of one methyl group. Such cavities are too small and hydrophobic to be filled with water, and the energetic cost of the resulting vacuum is presumably responsible for the loss of affinity (Eriksson et al., 1992). A9M abrogates binding by the opposite principle,

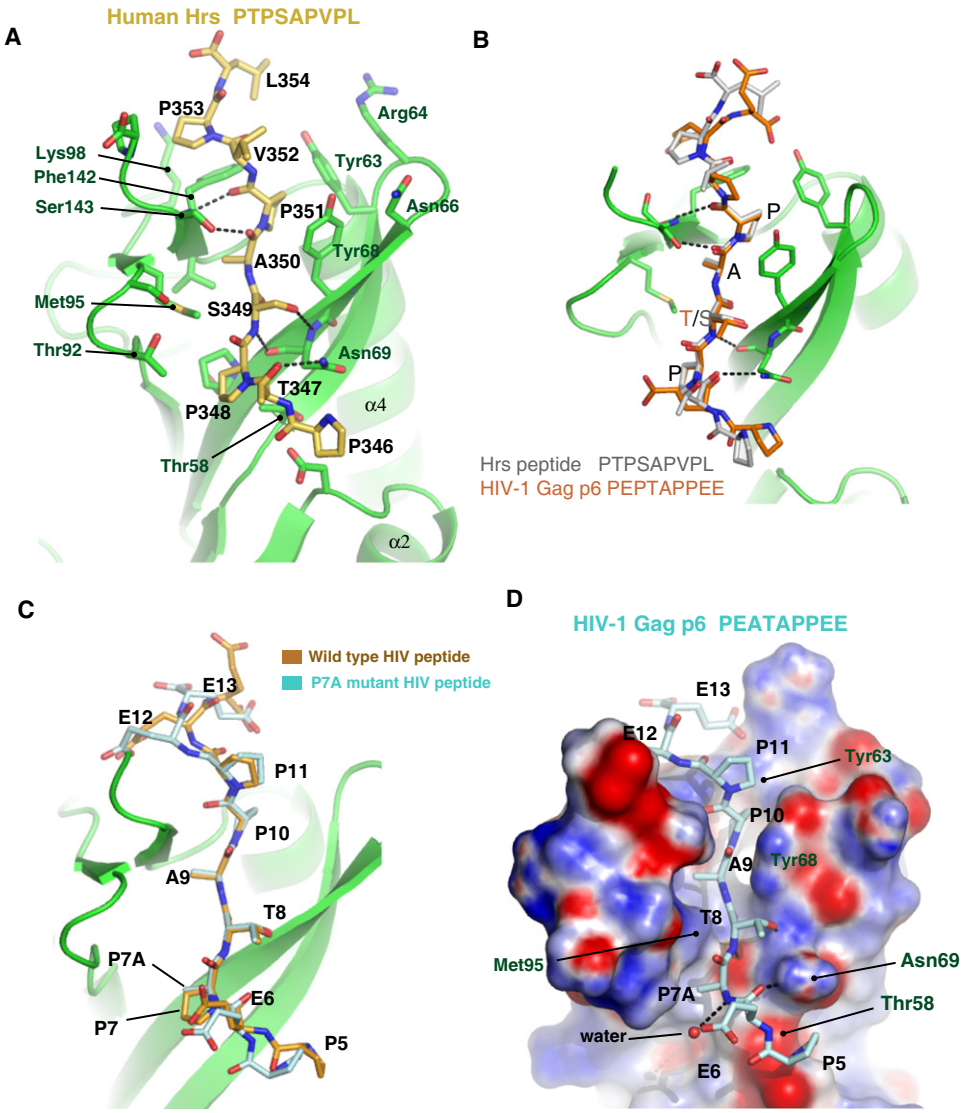

Figure 3. Recognition of HRS and HIV-1 Peptides by UEV Domain

(A) Binding of HRS peptide on UEV domain.

(B) Structural superposition of HRS and HIV p6 peptides.

(C) Superposition of the wild-type HIV-1 p6 peptide and the P7A mutant peptide.

(D) Surface representation of the UEV-P7A peptide binding.

introducing a steric collision into the binding site (Figure 4B and Table 2). Consistent with expectation, HIV-1 nonapeptide mutants T8A and P10A had no detectable binding (Figure 4B and Table 2).

Finally, we evaluated the effects of altering the less conserved residues at the start of and surrounding the HIV-1 PTAP motif. Pro7 is not as critical for binding as the other residues in the PTAP motif (Schlundt et al., 2009), and both P7A and P7S mutants were tested (Figure 4B and Table 2). The P7A mutant leads to a less than 3-fold reduction in affinity, consistent with the results of Schlundt et al. (2009). Indeed, Pro7 buries 86 $Å^2$ of solvent accessible surface area in the UEV domain interface, compared with 115 $Å^2$ for the more critical Pro10. The P7S mutant was designed on the basis of an observation by one of us (X.R., unpublished data) that the central region of Hrs can bind to the UEV domain even when the Hrs PSAP region is deleted. This region contains two SSAP sequences. The finding that P7S has measurable binding explains how this sequence is able to bind to the UEV domain in the absence of an intact PSAP motif. The P11A peptide was made to investigate the role of this residue, which is replaced by a Val in the Hrs sequence. P11A has a K_d greater by a factor of 3.5 as compared with wild-type (Figure 4B and Table 2). Indeed, the affinity of P11A, which does not inhibit HIV-1 budding (Demirov et al., 2002b), for the UEV domain is similar to that of the Hrs nonapeptide itself, which is 6-fold lower than that of the wild-type HIV-1 nonapeptide (Figure 4B and Table 2). The 6-fold affinity difference between HIV-1 Gag and

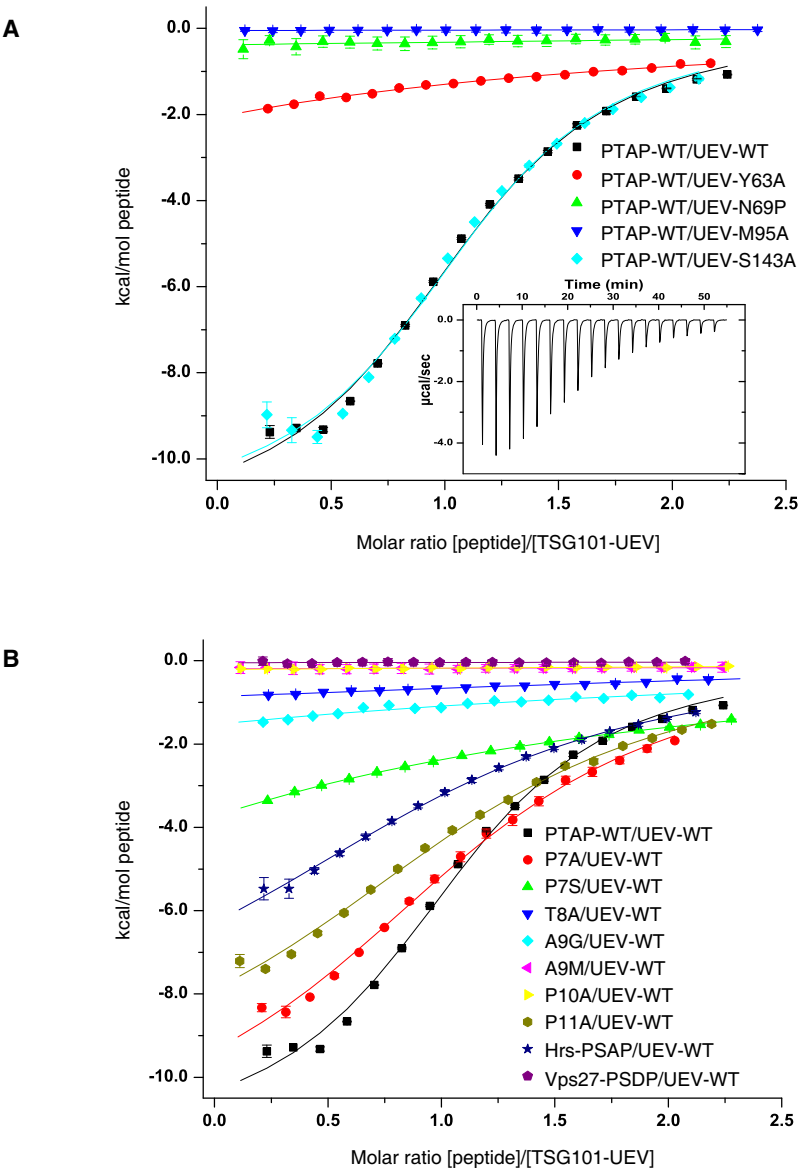

Figure 4. Isothermal Titration Calorimetry (ITC) of the UEV-P(S/T)AP Interaction

(A) Binding of Gag PTAP peptide to wild-type and mutant TSG101 UEV domains. The inset showed the differential heat released when Gag PTAP peptide (0.38 mM) was injected into the TSG101 UEV wild-type solution (4 mM) in 2.1 μl aliquots.

(B) ITC measurement of the binding of Gag PTAP wild-type and mutant peptides to TSG101 UEV domain. Error bars represent the standard deviation of three measurements.

Hrs peptides is nearly identical to the 7-fold difference reported previously (Pornillos et al., 2003). A corresponding peptide from Vps27, which is the yeast counterpart of Hrs, and has an analogous interaction with yeast ESCRT-I, does not bind to the human UEV domain, however. Taken together, these results show consistency with the structural findings, sequence conservation, and previous in vitro quantitative and library-based binding analyses, and add to the tools available to probe function in vivo.

Gag PTAP Motif Binding to TSG101 Is Required for HIV-1 Release

To measure the effect of TSG101 PTAP-binding site mutations on HIV-1 release, metabolic radio-immunoprecipitation of cells expressing WT HIV-1 was performed. In the control cultures, HeLa cells were transfected with nontargeting siRNA and relative virus release efficiency was set to 100%. Knockdown of TSG101 resulted in a ~5-fold reduction in virus release efficiency (Figure 5A). The budding defect induced by TSG101 depletion was also accompanied by the characteristic (Gottlinger et al., 1991; Huang et al., 1995) accumulation of the p25 processing intermediate relative to mature p24 (CA) (see p25 to p24 levels in the cell-associated panel of Figure 5). The virus release defect induced by TSG101 depletion could be rescued by providing exogenous, siRNA-resistant TSG101, such that the virus release efficiency was restored to ~80% that of the control. Mutations in the TSG101 UEV domain at positions Y63, N69, and M95 abrogated the ability of the siRNA-resistant TSG101 to rescue virus release (Figure 5B). The essentially complete lack of rescue is consistent with the complete loss of binding observed by ITC. The transfection efficiencies of the Y63, N69, and M95 mutant expression vectors were comparable to those of the WT, and even at high DNA input levels these three mutants failed to rescue virus release in Tsg101-depleted cells (data not shown). The S143A mutant partially rescued virus release, to levels approximately 2-fold that observed in the control cultures. The partial effect of the S143A mutant on virus release strikingly illustrates the sensitivity of virus release to small perturbations in affinity, given that the effects of this mutation on equilibrium binding in vitro are marginal.

Hrs PSAP Motif Binding to TSG101 Is Not Required for EGFR Downregulation

In order to probe the role of the P(S/T)AP motif binding site on the TSG101 UEV domain in receptor downregulation, endogenous *TSG101* was silenced in HeLa cells as described above. Rescue constructs encoding wild-type TSG101 and the four mutants assessed above were tested for function. Following 60 min stimulation of serum-starved cells with 50 or 100 ng/ml EGF, EGFR levels dropped sharply in cells not treated with siRNA (Figure 6A). Knockdown of TSG101 prevented the decrease in EGFR levels upon treatment with EGF (Figure 6B and second lane of Figure 6C). This result demonstrated that TSG101 depletion blocked ESCRT-mediated turnover of activated EGFR.

Table 2. Equilibrium Dissociation Constants for the Various ITC Experiments.

UEV	Peptide name	Peptide sequence	K_D (μM)
UEV-WT	Gag PTAP-WT	$_5$PEPTAPPEE$_{13}$	50 ± 0.7
UEV-WT	P7A	PEATAPPEE	130 ± 4.0
UEV-WT	P7S	PESTAPPEE	1600 ± 14
UEV-WT	T8A	PEPAAPPEE	N.B.
UEV-WT	A9G	PEPTGPPEE	N.B.
UEV-WT	A9M	PEPTMPPEE	N.B.
UEV-WT	P10A	PEPTAAPEE	N.B.
UEV-WT	P11A	PEPTAPAEE	170 ± 15
UEV-WT	HRS-PSAP	PTPSAPVPL	290 ± 42
UEV-WT	Vps27-PSDP	LAPSDPPYP	N.B.
UEV-Y63A	Gag PTAP-WT	PEATAPPEE	N.B.
UEV-N69P	Gag PTAP-WT	PEATAPPEE	N.B.
UEV-M95A	Gag PTAP-WT	PEATAPPEE	N.B.
UEV-S143A	Gag PTAP-WT	PEATAPPEE	53 ± 2.8

N.B., no binding.

The effects of TSG101 knockdown were completely reversed by transfection of the siRNA-resistant allele (WT-R, third lane in Figure 6C). Each of the mutant constructs was then tested (lanes 4–7, Figure 6C). The TSG101 mutants were as effective as the wild-type in rescuing the effect of the knockdown, demonstrating that they retained full function in EGFR downregulation.

DISCUSSION

The high-resolution crystal structures of TSG101 UEV domain-peptide complexes, together with in vitro binding studies and previous work, provide a richly detailed picture of the binding determinants for the human TSG101 UEV domain. If the second Pro is defined as the "most important" residue for reference purposes and numbered "0" (Aasland et al., 2002), the minimal required motif would be Pro/Ala at –3, Ser/Thr at –2, Ala at –1, and Pro at 0. The "preferred" motif would additionally have a Pro at +1. These determinants are set by well-defined hydrophobic pockets, as described here and previously (Pornillos et al., 2002a), together with the hydrogen-bonding network described in this study. Regarding the importance of the Pro at +1, alignment of PT/SAP motifs from diverse enveloped viruses indicates that the presence of a Pro at this position is highly, but not absolutely, conserved. The final (+1) Pro in the P(S/T)APP motif is found across all major clades of HIV-1 and is also found in HIV-2, SIVagm SIVcpz, SIVgor, and SIVsmm (http://www.hiv.lanl.gov/content/sequence/HIV/COMPENDIUM/2010/plvprot.pdf). Visna

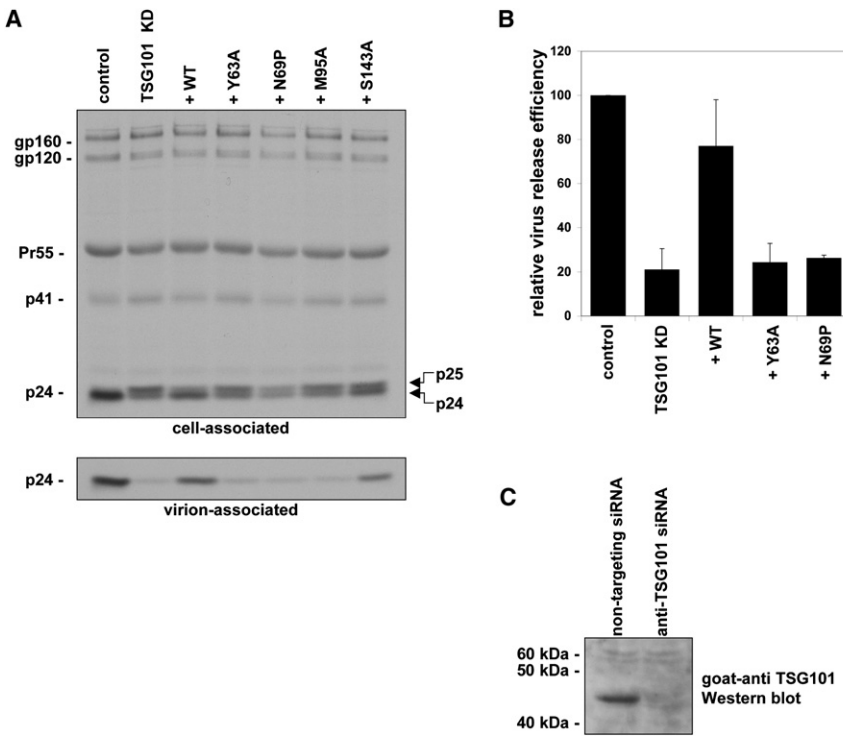

Figure 5. Mutation of the TSG101 UEV Domain Disrupts HIV-1 Release

(A) HeLa cells were transfected with anti-TSG101 siRNA to knock down endogenous Tsg101 expression, and 24 hr later were cotransfected with the HIV-1 molecular clone pNL4-3 and vectors expressing siRNA-resistant WT or mutant TSG101 as indicated. Cells were metabolically labeled with [^{35}S]Met/Cys and cell and virus lysates were immunoprecipitated with anti-HIV-1 Ig. Cell-associated and virion-associated immunoprecipitates were quantitated by autoradiography.

(B) Relative virus release efficiency calculated as p24 (CA) in the virus supernatant divided by total Gag protein in the cell and virus. Error bars indicate SD from three independent experiments.

(C) Anti-TSG101 western blot, demonstrating efficient depletion of endogenous TSG101 protein levels.

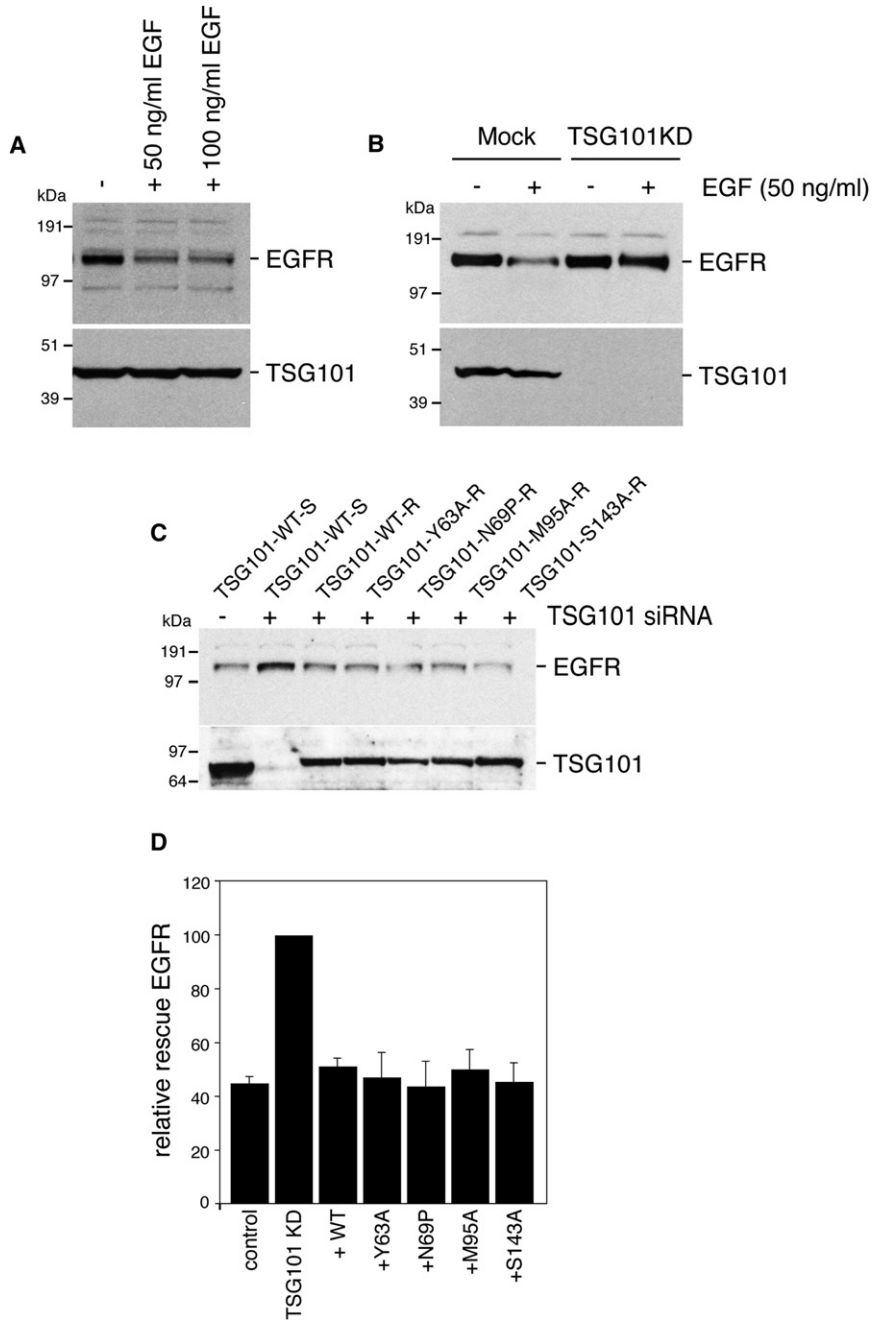

Figure 6. A Functional PTAP Binding Site in TSG101 Is Not Needed for EGFR Downregulation

(A) HeLa cells were starved in serum-free medium for 1 hr at 37°C and then incubated with EGF (50 or 100 ng/ml) for 1 hr at 37°C. Protein extracts were analyzed by immunoblotting with a polyclonal antibody to EGFR (RK-2) and a monoclonal antibody to TSG101.

(B) After a 72 hr treatment with TSG101 siRNAi, cells were starved in serum-free medium for 1 hr at 37°C and then incubated with 50 ng/ml EGF for 1 hr at 37°C. Mock and TSG101KD extracts were analyzed by immunoblotting for EGFR and TSG101.

(C) After a 48 hr treatment with TSG101 siRNAi, cells were transfected with TSG101 constructs (rescue). At 20 hr posttransfection, cells were starved in serum-free medium for 1 hr at 37°C and then incubated with 50 ng/ml EGF for 1 hr at 37°C. Extracts were analyzed by immunoblotting for EGFR and GFP-TSG101 with a polyclonal antibody to GFP. Transfection efficiency was higher than 50% in each experiment confirmed by fluorescence microscopy visualizing cells expressing GFP-TSG101.

(D) Levels of EGFR were quantitated by X-ray film densitometry and percentages of undegraded EGFR upon EGF induction were plotted. Bars represent the mean ± SD from three independent experiments.

virus, bovine immunodeficiency virus, and feline immunodeficiency virus all encode P(S/T)APP motifs, as does Ebola virus, whereas in HTLV-1 this motif is PTAPQ. We have studied the effects of mutating the +1 Pro in HIV-1 (Demirov et al., 2002b) and find that while particle budding occurs efficiently upon PTAPP to PTAPE mutation, the Gag processing intermediate p41 accumulates, suggesting a delay in budding kinetics.

The ability of HIV-1 to rapidly develop resistance to drugs has leant urgency to the discovery of alternative therapeutic targets. From the initial discovery of the HIV-1 Gag PTAP-TSG101 interaction, ESCRT-I has appeared to be one of the more critical host-pathogen interactors in the HIV life cycle, and thus a promising target. However, efforts at developing PTAP inhibitors have suffered to some extent from the impression that such inhibitors might also interfere with the downregulation of proliferative receptors such as EGFR and thus promote tumorigenesis. The most influential study along these lines was based on antisense inhibition of TSG101 and rescue with UEV domain mutants that included the Y63A and M95A mutants also studied here (Lu et al., 2003). In the Lu et al. report, downregulation of transfected EGFR was monitored following prolonged (90 min) stimulation with very high levels (150 ng/ml) of EGF. The Lu et al. study does establish that PSAP recognition by the UEV is required under at least some conditions. We infer that PSAP recognition is likely to be at least involved, if not required, under other conditions. In the current study, endogenous EGFR was monitored following treatment with 50–100 ng/ml EGF for 60 min, which is at the high end of the range conventionally used in EGFR degradation assays. These results suggest to us that under normal or even moderately intense stimulatory conditions, the Hrs PSAP-TSG101 UEV interaction is not rate limiting, although it may become rate limiting under conditions of exceptionally intense loading with highly stimulated exogenous receptors. The results

in this study are consistent with the previous observation that overexpression of the TSG101 UEV domain fragment, which potently blocks HIV-1 budding, does not inhibit EGFR degradation (Demirov et al., 2002a).

The interaction between TSG101 UEV and Hrs PSAP is not required for EGFR downregulation under normal conditions, even though TSG101 (Babst et al., 2000; Lu et al., 2003) and Hrs (Bishop et al., 2002; Chin et al., 2001; Lu et al., 2003) are required individually. The yeast counterparts of TSG101 and Hrs are the Vps23 and Vps27 subunits of ESCRT-I and ESCRT-0, respectively. ESCRT-0 is responsible for organizing ubiquitinated proteins into clusters on the endosomal membrane, while ESCRT-I cooperates with ESCRT-II to create buds into which the ubiquitinated cargo are sorted (Wollert and Hurley, 2010). Loss of the PSDP motifs in yeast ESCRT-0 that are required to bind to yeast ESCRT-I reduces, but does not completely eliminate, colocalization of ESCRT-I and -II (Wollert and Hurley, 2010). Residual colocalization could be mediated by some other part of the structures, or by an indirect effect such as lipid or cargo clustering. Indeed, there have been several reports suggesting that other parts of the ESCRT-0 and -I complexes interact with one another (Bouamr et al., 2007; Eastman et al., 2005; Stuchell et al., 2004). It seems likely that PSAP-mediated colocalization of human ESCRT-0 and ESCRT-I does occur during normal EGFR sorting, but is not the rate-determining step, and therefore disrupting PSAP-TSG101 binding has no effect on EGFR downregulation. It is currently unknown what the role of this interaction is in downregulation of other cell surface proteins.

In summary, the results described here provide clear-cut validation for the concept that HIV-1 budding inhibitors targeted at the PTAP binding site of human TSG101 will not necessarily disrupt certain host functions, such as EGFR downregulation. The ESCRT system has other host functions in addition to receptor downregulation, such as cytokinesis (McDonald and Martin-Serrano, 2009), but Hrs is not currently thought to have a role in this pathway. Nevertheless, the M95A mutant of TSG101 has been reported to have a partial cytokinesis phenotype (Carlton and Martin-Serrano, 2007), and the possibility of PTAP inhibitor effects on cytokinesis is a concern that still needs to be addressed. Inhibitor design efforts, whether through purely in silico screening or through the use of structural analysis as an adjunct to traditional medicinal chemistry approaches, stand to benefit from having the most accurate possible structures of the target complexes. The structures reported here, at up to 1.4 Å resolution, provide the first accurate details of the hydrogen-bonding network in the PTAP binding site and should be an important addition to the PTAP inhibitor design toolkit.

EXPERIMENTAL PROCEDURES

Protein Expression and Purification

DNA coding for the human TSG101 UEV domain (residues 2–145) was subcloned into the pGST2 vector (Sheffield et al., 1999). Tsg101 UEV was tagged with an N-terminal GST followed by a tobacco etch virus (TEV) protease cleavage site. In order to improve the crystallization properties of the UEV domain, 6 residues (residues 43–48, VFNDGS) in the β1-β2 loop were mutated to Gly-Thr-Gly. The plasmid was transformed into *Escherichia coli* strain BL21 (DE3) Star and expressed overnight at 30°C. Cells were resuspended in 1X PBS buffer and lysed by sonication. The GST-UEV was isolated using glutathione affinity chromatography. The eluate was concentrated and the GST tag was removed by cleavage with TEV protease. The UEV domain was further purified by Superdex S200 size exclusion chromatography. The fractions containing the UEV domain concentrated to 10 mg/ml in buffer 10 mM Tris-HCl (pH 8.0), 100 mM NaCl for crystallization.

General Procedure for Solid-Phase Peptide Synthesis

Peptides were synthesized on NovaSynTGR resin (Novabiochem, cat. no. 01-64-0060) or Rink Amide MBHA resin (Novabiochem, cat. no. 01-64-0037) by standard Fmoc solid-phase protocols using active ester coupling methodology in *N*,*N*-dimethylforamide (DMF). In summary for each residue, amino acid (5.0 equivalents based on resin loading), 1-hydroxybenzotriazole (HOBT) (5.0 eq.) and *N,N'*-diisopropylcarbodiimide (DIC) (5.0 eq.) was used for primary amines (single couple, 2 hr) and bromo-tris-pyrrolidino-phosphonium hexafluorophosphate (PyBroP) (5.0 eq.) and diisopropylethylamine (DIEA) (10.0 eq.) (double coupling; 2 hr each) was employed for secondary amines. The amino terminus was acetylated using acetic anhydride (10.0 eq.) in DMF. The final resin was washed with DMF, methanol, dichloromethane, and ether and then dried under vacuum (overnight). Peptides were cleaved from the resin (200 mg) by treatment with trifluoroacetic acid: triisopropylsilane: H_2O (90: 5: 5) (5 ml, 4 hr). The resin was removed by filtration and the filtrate was concentrated in vacuo, and the peptide was then precipitated by the addition of cold ether and the precipitate was washed with ether. The resulting white solid was dissolved in 50% aqueous acetonitrile (5 ml) and purified by reverse phase preparative HPLC using a Phenomenex C_{18} column (21 mm dia x 250 mm, cat. no: 00G-4436-P0) with a linear gradient from 0% aqueous acetonitrile (0.1% trifluoroacetic acid) to 50% acetonitrile (0.1% trifluoroacetic acid) over 35 min at a flow rate of 10.0 ml/minute (detection at 220 nm). Lyophilization provided products as white powders. The purity of final peptides was determined by HPLC using a Waters Corp. XBridgeTM BEH130 C_{18} column (Part no: 186003581) (4.60 mm dia × 250 mm, 5 μm) at a flow rate of 1.0 ml/minute. Electrospray ionization-mass spectra (ESIMS) were acquired with an Agilent LC/MS system and Matrix-assisted laser desorption/ionization (MALDI) mass spectra were acquired with Shimadzu Biotech Axima instrument using α–cyano-4-hydroxycinnamic acid as matrix. High-resolution mass spectra (HRMS) were obtained from the UCR Mass Spectrometry Facility, University of California at Riverside.

Crystallization and Crystallographic Analysis

Crystals of UEV-HIV-1 Gag nonapeptide complex were grown by vapor-diffusion methods at 25°C over a reservoir of 100 mM HEPES-NaOH (pH 7.5), 25% PEG 3350, 200 mM $NaNO_3$ for 1 week. Crystals were cryoprotected in Paratone and flash frozen using liquid nitrogen. Native data were collected from a single frozen crystal with an MAR CCD detector at beamline 22-ID and 22-BM, APS. All data were processed and scaled using HKL2000 (HKL Research). The structure of the complex was determined by molecular replacement with the program PHASER (McCoy et al., 2007) using the 2.26 Å crystal structure of the unliganded human TSG101 UEV domain (PDB code: 2F0R) (Palencia et al., 2006) as a starting model. The initial model of UEV peptide was built into the density-modified map using the programs Coot (Emsley and Cowtan, 2004). The refinement was carried out using CNS (Brunger et al., 1998) with anisotropic B factor refinement. The final model consisted of one copy of UEV domain and the peptide. There are no residues in disallowed region of the Ramachandran plot. Structures of the complexes with the Hrs nonapeptide and the HIV-1 Gag P7A mutant peptide, as well as the $P2_1$ crystal form of the unliganded UEV domain were obtained and solved as above. All structural figures were prepared using the program PyMOL (W. Delano, http://pymol.sourceforge.net/).

Isothermal Titration Calorimetry

Purified wild-type and mutant TSG101 UEV domains were dialyzed against the ITC buffer (20 mM sodium phosphate [pH 7.20] 150 mM NaCl, and 5% glycerol) overnight at 4°C. Peptides were dissolved in the same ITC buffer. All ITC experiments were carried out at 28°C on an ITC_{200} instrument (MicroCal LLC, Northampton, MA). The sample cell contained 0.2 ml of 300–600 μM UEV proteins and the peptides (4 or 6.5 mM) were added in 18 injections of 2.1 μl each. Data from peptide injections into buffer blanks were subtracted

from sample data before analysis. The data were processed using Origin software (MicroCal). The binding constant (K_d) was fitted as a one-site model.

Rescue Constructs and siRNAs

The full-length HIV-1 molecular pNL4-3 (Adachi et al., 1986) was used to produce infectious virus in HeLa cells. The siRNA-resistant pIRES2-GFP-TSG101* (Garrus et al., 2001) was a kind gift from W. Sundquist (University of Utah). Point mutations in the TSG101 UEV domain were introduced in this plasmid by site-directed mutagenesis. The anti-TSG101 siRNA corresponds to the target sequence: 5′-AACCTCCAGTCTTCTCTCGTC-3′.

Virus Release Assay

HeLa cells were cultured in Dulbecco's modified Eagle medium with 5% fetal bovine serum. Anti-TSG101 siRNAs were transfected into HeLa cells with Lipofectamine RNAiMax reagent (Invitrogen). Twenty-four hours after siRNA transfection, cells were transfected again with anti-TSG101 siRNA and pNL4-3 and the siRNA-resistant TSG101 expression plasmids using Lipofectamine 2000 (Invitrogen). HIV-1 particle release assays were performed as previously described (Freed and Martin, 1994; Willey et al., 1988). In brief, transfected cells were starved for 30 min in medium devoid of L-methionine, L-cysteine, and fetal bovine serum. Cells were then labeled with [^{35}S]Cys/Met Protein Express Labeling Mix (Perkin Elmer) for 3 hr. Virions were isolated from the virus supernatant by ultracentrifugation for 1 hr at 45,000 rpm. Virus and cell lysates were prepared in 0.5% Triton X-100 lysis buffer. Virus and cell lysates were immunoprecipitated with HIV-1 Ig (NIH AIDS Reference Reagent Program). Radioimmunoprecipitates were resolved by SDS-PAGE followed by autoradiography and phosphorimager quantitation. Western blotting was performed on cell lysates using goat polyclonal anti-TSG101 (Santa Cruz, sc-6037).

EGFR Downregulation Assay

At 48 hr post-RNAi transfection, HeLa cells were transfected with plasmids encoding siRNA-sensitive or resistant forms of GFP-TSG101–FLAG (WT or Y63A, N69P, M95A, S143A mutants). At 20 hr posttransfection, cells were starved in serum-free medium for 1 hr and then incubated with 50–100 ng/ml EGF (Upstate) at 37°C for 60 min. Cells were then washed with cold PBS and immediately lysed. Lysates were subjected to SDS/PAGE and immunoblotting using a polyclonal antibody to the EGFR (RK-2, a gift from Joseph Schlessinger, Yale University) and a polyclonal antibody to GFP (Invitrogen).

ACCESSION NUMBERS

Crystallographic coordinates have been deposited in the Protein Data Bank with the accession codes 3OBQ, 3OBS, 3OBU, and 3OBX.

ACKNOWLEDGMENTS

We thank M. Stewart for technical assistance, W. Sundquist for the siRNA-resistant TSG101 expression vector, J. Schlessinger for an antibody, and G. Mardones for discussions. GM/CA CAT has been funded in whole or in part with federal funds from the NCI (Y1-CO-1020) and the NIGMS (Y1-GM-1104). Use of the Advanced Photon Source was supported by the U.S. Department of Energy, Basic Energy Sciences, Office of Science, under contract No. DE-AC02-06CH11357. This work was supported by the NIDDK, NCI, NICHD, and IATAP programs of the NIH intramural research program. Y.J.I. and X.R. were supported in part by NIH Intramural AIDS Research Fellowships.

Received: July 14, 2010
Revised: July 14, 2010
Accepted: August 6, 2010
Published: November 9, 2010

REFERENCES

Aasland, R., Abrams, C., Ampe, C., Ball, L.J., Bedford, M.T., Cesareni, G., Gimona, M., Hurley, J.H., Jarchau, T., Lehto, V.P., et al. (2002). Normalization of nomenclature for peptide motifs as ligands of modular protein domains. FEBS Lett. *513*, 141–144.

Adachi, A., Gendelman, H.E., Koenig, S., Folks, T., Willey, R., Rabson, A., and Martin, M.A. (1986). Production of acquired immunodeficiency syndrome-associated retrovirus in human and nonhuman cells transfected with an infectious molecular clone. J. Virol. *59*, 284–291.

Audhya, A., McLeod, I.X., Yates, J.R., and Oegama, K. (2007). MVB-12, a fourth subunit of metazoan ESCRT-I, functions in receptor downregulation. PLoS ONE *2*, e956. 10.1371/journal.pone.0000956.

Babst, M., Odorizzi, G., Estepa, E.J., and Emr, S.D. (2000). Mammalian tumor susceptibility gene 101 (TSG101) and the yeast homologue, Vps23p, both function in late endosomal trafficking. Traffic *1*, 248–258.

Bache, K.G., Brech, A., Mehlum, A., and Stenmark, H. (2003). Hrs regulates multivesicular body formation via ESCRT recruitment to endosomes. J. Cell Biol. *162*, 435–442.

Bieniasz, P.D. (2009). The cell biology of HIV-1 virion genesis. Cell Host Microbe *5*, 550–558.

Bishop, N., Horman, A., and Woodman, P. (2002). Mammalian class E vps proteins recognize ubiquitin and act in the removal of endosomal protein-ubiquitin conjugates. J. Cell Biol. *157*, 91–101.

Bouamr, F., Houck-Loomis, B.R., De Los Santos, M., Casaday, R.J., Johnson, M.C., and Goff, S.P. (2007). The C-terminal portion of the Hrs protein interacts with Tsg101 and interferes with human immunodeficiency virus type 1 Gag particle production. J. Virol. *81*, 2909–2922.

Brunger, A.T., Adams, P.D., Clore, G.M., DeLano, W.L., Gros, P., Grosse-Kunstleve, R.W., Jiang, J.S., Kuszewski, J., Nilges, M., Pannu, N.S., et al. (1998). Crystallography & NMR system: a new software suite for macromolecular structure determination. Acta Crystallogr. D Biol. Crystallogr. *54*, 905–921.

Carlton, J.G., and Martin-Serrano, J. (2007). Parallels between cytokinesis and retroviral budding: a role for the ESCRT machinery. Science *316*, 1908–1912.

Chen, B.J., and Lamb, R.A. (2008). Mechanisms for enveloped virus budding: Can some viruses do without an ESCRT? Virology *372*, 221–232.

Chin, L.S., Raynor, M.C., Wei, X.L., Chen, H.Q., and Li, L. (2001). Hrs interacts with sorting nexin 1 and regulates degradation of epidermal growth factor receptor. J. Biol. Chem. *276*, 7069–7078.

Demirov, D.G., Ono, A., Orenstein, J.M., and Freed, E.O. (2002a). Overexpression of the N-terminal domain of TSG101 inhibits HIV-1 budding by blocking late domain function. Proc. Natl. Acad. Sci. USA *99*, 955–960.

Demirov, D.G., Orenstein, J.M., and Freed, E.O. (2002b). The late domain of human immunodeficiency virus type 1 p6 promotes virus release in a cell type-dependent manner. J. Virol. *76*, 105–117.

Eastman, S.W., Martin-Serrano, J., Chung, W., Zang, T., and Bieniasz, P.D. (2005). Identification of human VPS37C, a component of endosomal sorting complex required for transport-I important for viral budding. J. Biol. Chem. *280*, 628–636.

Emsley, P., and Cowtan, K. (2004). Coot: model-building tools for molecular graphics. Acta Crystallogr. D Biol. Crystallogr. *60*, 2126–2132.

Eriksson, A.E., Baase, W.A., Zhang, X.J., Heinz, D.W., Blaber, M., Baldwin, E.P., and Matthews, B.W. (1992). Response of a protein-structure to cavity-creating mutations and its relation to the hydrophobic effect. Science *255*, 178–183.

Freed, E.O. (2002). Viral late domains. J. Virol. *76*, 4679–4687.

Freed, E.O., and Martin, M.A. (1994). Evidence for a functional interaction between the V1/V2 and C4 domains of human immunodeficiency virus type 1 envelope glycoprotein gp120. J. Virol. *68*, 2503–2512.

Garrus, J.E., von Schwedler, U.K., Pornillos, O.W., Morham, S.G., Zavitz, K.H., Wang, H.E., Wettstein, D.A., Stray, K.M., Cote, M., Rich, R.L., et al. (2001). Tsg101 and the vacuolar protein sorting pathway are essential for HIV-1 budding. Cell *107*, 55–65.

Gottlinger, H.G., Dorfman, T., Sodroski, J.G., and Haseltine, W.A. (1991). Effect of mutations affecting the P6 Gag protein on human-immunodeficiency-virus particle release. Proc. Natl. Acad. Sci. USA *88*, 3195–3199.

Huang, M., Orenstein, J.M., Martin, M.A., and Freed, E.O. (1995). P6(Gag) is required for particle-production from full-length human-immunodeficiency-virus type-1 molecular clones expressing protease. J. Virol. *69*, 6810–6818.

Hurley, J.H., and Hanson, P.I. (2010). Membrane budding and scission by the ESCRT complexes: it's all in the neck. Nat. Rev. Mol. Cell Biol. *11*, 556–566.

Kostelansky, M.S., Schluter, C., Tam, Y.Y.C., Lee, S., Ghirlando, R., Beach, B., Conibear, E., and Hurley, J.H. (2007). Molecular architecture and functional model of the complete yeast ESCRT-I heterotetramer. Cell *129*, 485–498.

Li, L., and Cohen, S.N. (1996). Tsg101: A novel tumor susceptibility gene isolated by controlled homozygous functional knockout of allelic loci in mammalian cells. Cell *85*, 319–329.

Liu, F., Stephen, A.G., Waheed, A.A., Aman, M.J., Freed, E.O., Fisher, R.J., and Burke, T.R. (2008). SAR by oxime-containing peptide libraries: application to Tsg101 ligand optimization. ChemBioChem *9*, 2000–2004.

Lu, Q., Hope, L.W.Q., Brasch, M., Reinhard, C., and Cohen, S.N. (2003). TSG101 interaction with HRS mediates endosomal trafficking and receptor down-regulation. Proc. Natl. Acad. Sci. USA *100*, 7626–7631.

Luttge, B.G., Shehu-Xhilaga, M., Demirov, D.G., Adamson, C.S., Soheilian, F., Nagashima, K., Stephen, A.G., Fisher, R.J., and Freed, E.O. (2008). Molecular characterization of feline immunodeficiency virus budding. J. Virol. *82*, 2106–2119.

Martin-Serrano, J., Zang, T., and Bieniasz, P.D. (2001). HIV-I and Ebola virus encode small peptide motifs that recruit Tsg101 to sites of particle assembly to facilitate egress. Nat. Med. *7*, 1313–1319.

McCoy, A.J., Grosse-Kunstleve, R.W., Adams, P.D., Winn, M.D., Storoni, L.C., and Read, R.J. (2007). Phaser crystallographic software. J. Appl. Crystallogr. *40*, 658–674.

McDonald, B., and Martin-Serrano, J. (2009). No strings attached: the ESCRT machinery in viral budding and cytokinesis. J. Cell Sci. *122*, 2167–2177.

Moberg, K.H., Schelble, S., Burdick, S.K., and Hariharan, I.K. (2005). Mutations in erupted, the Drosophila ortholog of mammalian tumor susceptibility gene 101, elicit non-cell-autonomous overgrowth. Dev. Cell *9*, 699–710.

Morita, E., and Sundquist, W.I. (2004). Retrovirus budding. Annu. Rev. Cell Dev. Biol. *20*, 395–425.

Morita, E., Sandrin, V., Alam, S.L., Eckert, D.M., Gygi, S.P., and Sundquist, W.I. (2007). Identification of human MVB12 proteins as ESCRT-I subunits that function in HIV budding. Cell Host Microbe *2*, 41–53.

Palencia, A., Martinez, J.C., Mateo, P.L., Luque, I., and Camara-Artigas, A. (2006). Structure of human TSG101 UEV domain. Acta Crystallogr. D Biol. Crystallogr. *62*, 458–464.

Pornillos, O., Alam, S.L., Davis, D.R., and Sundquist, W.I. (2002a). Structure of the Tsg101 UEV domain in complex with the PTAP motif of the HIV-1 p6 protein. Nat. Struct. Biol. *9*, 812–817.

Pornillos, O., Alam, S.L., Rich, R.L., Myszka, D.G., Davis, D.R., and Sundquist, W.I. (2002b). Structure and functional interactions of the Tsg101 UEV domain. EMBO J. *21*, 2397–2406.

Pornillos, O., Higginson, D.S., Stray, K.M., Fisher, R.D., Garrus, J.E., Payne, M., He, G.P., Wang, H.E., Morham, S.G., and Sundquist, W.I. (2003). HIV Gag mimics the Tsg101-recruiting activity of the human Hrs protein. J. Cell Biol. *162*, 425–434.

Raiborg, C., and Stenmark, H. (2009). The ESCRT machinery in endosomal sorting of ubiquitylated membrane proteins. Nature *458*, 445–452.

Schlundt, A., Sticht, J., Piotukh, K., Kosslick, D., Jahnke, N., Keller, S., Schuemann, M., Krause, E., and Freund, C. (2009). Proline-rich sequence recognition. II. Proteomics analysis of Tsg101 ubiquitin-E2-like variant (UEV) interactions. Mol. Cell. Proteomics *8*, 2474–2486.

Shafer, R.W., and Schapiro, J.M. (2008). HIV-1 drug resistance mutations: an updated framework for the second decade of HAART. AIDS Rev. *10*, 67–84.

Sheffield, P., Garrard, S., and Derewenda, Z. (1999). Overcoming expression and purification problems of RhoGDI using a family of "parallel" expression vectors. Protein Expr. Purif. *15*, 34–39.

Stuchell, M.D., Garrus, J.E., Muller, B., Stray, K.M., Ghaffarian, S., McKinnon, R., Krausslich, H.G., Morham, S.G., and Sundquist, W.I. (2004). The human endosomal sorting complex required for transport (ESCRT-I) and its role in HIV-1 budding. J. Biol. Chem. *279*, 36059–36071.

Sundquist, W.I., Schubert, H.L., Kelly, B.N., Hill, G.C., Holton, J.M., and Hill, C.P. (2004). Ubiquitin recognition by the human TSG101 protein. Mol. Cell *13*, 783–789.

Tavassoli, A., Lu, Q., Gam, J., Pan, H., Benkovic, S.J., and Cohen, S.N. (2008). Inhibition of HIV budding by a genetically selected cyclic peptide targeting the Gag-TSG101 interaction. ACS Chem. Biol. *3*, 757–764.

Teo, H., Veprintsev, D.B., and Williams, R.L. (2004). Structural insights into endosomal sorting complex required for transport (ESCRT-I) recognition of ubiquitinated proteins. J. Biol. Chem. *279*, 28689–28696.

VerPlank, L., Bouamr, F., LaGrassa, T.J., Agresta, B., Kikonyogo, A., Leis, J., and Carter, C.A. (2001). Tsg101, a homologue of ubiquitin-conjugating (E2) enzymes, binds the L domain in HIV type 1 Pr55(Gag). Proc. Natl. Acad. Sci. USA *98*, 7724–7729.

Waheed, A.A., and Freed, E.O. (2008). Peptide inhibitors of HIV-1 egress. ACS Chem. Biol. *3*, 745–747.

Willey, R.L., Bonifacino, J.S., Potts, B.J., Martin, M.A., and Klausner, R.D. (1988). Biosynthesis, cleavage, and degradation of the human immunodeficiency virus 1 envelope glycoprotein gp160. Proc. Natl. Acad. Sci. USA *85*, 9580–9584.

Wollert, T., and Hurley, J.H. (2010). Molecular mechanism of multivesicular body biogenesis by the ESCRT complexes. Nature *464*, 864–869.

Wollert, T., Wunder, C., Lippincott-Schwartz, J., and Hurley, J.H. (2009). Membrane scission by the ESCRT-III complex. Nature *458*, 172–177.